

Topographically driven differences in energy and water constrain climatic control on forest carbon sequestration

TYSON L. SWETNAM,^{1,†} PAUL D. BROOKS,² HOLLY R. BARNARD,³ ADRIAN A. HARPOLD,⁴ AND ERIKA L. GALLO⁵

¹BIO5 Institute, University of Arizona, 1657 E Helen Street, Tucson, Arizona 85721 USA

²Department of Geology and Geophysics, University of Utah, Frederick Albert Sutton Building, 115 S 1460 E 383, Salt Lake City, Utah 84112 USA

³Department of Geography and INSTAAR, University of Colorado, Guggenheim 110, 260 UCB, Boulder, Colorado 80309 USA

⁴Department of Natural Resources and Environmental Science, University of Nevada, Reno, 1664 N. Virginia Street, Reno, Nevada 89557 USA

⁵Department of Hydrology and Water Resources, University of Arizona, JW Harshbarger Building 11, Tucson, Arizona 85721 USA

Citation: Swetnam, T. L., P. D. Brooks, H. R. Barnard, A. A. Harpold, and E. L. Gallo. 2017. Topographically driven differences in energy and water constrain climatic control on forest carbon sequestration. *Ecosphere* 8(4):e01797. 10.1002/ecs2.1797

Abstract. Mountains are vital to ecosystems and human society given their influence on global carbon and water cycles. Yet the extent to which topography regulates montane forest carbon uptake and storage remains poorly understood. To address this knowledge gap, we compared forest aboveground carbon loading to topographic metrics describing energy balance and water availability across three headwater catchments of the Boulder Creek Watershed, Colorado, USA. The catchments range from 1800 to 3500 m above mean sea level with 46–102 cm/yr mean annual precipitation and -1.2° to 12.3°C mean annual temperature. In all three catchments, we found mean forest carbon loading consistently increased from ridges (27 ± 19 Mg C ha) to valley bottoms (60 ± 28 Mg C ha). Low topographic positions held up to 185 ± 76 Mg C ha, more than twice the peak value of upper positions. Toe slopes fostered disproportionately high net carbon uptake relative to other topographic positions. Carbon storage was on average 20–40 Mg C ha greater on north to northeast aspects than on south to southwest aspects, a pattern most pronounced in the highest elevation, coldest and wettest catchment. Both the peak and mean aboveground carbon storage of the three catchments, crossing an 11°C range in temperature and doubling of local precipitation, defied the expectation of an optimal elevation-gradient climatic zone for net primary production. These results have important implications for models of forest sensitivity to climate change, as well as to predicted estimates of continental carbon reservoirs.

Key words: carbon; climate change; eco-hydrology; forests; lidar; microclimate; topography.

Received 22 March 2017; **accepted** 24 March 2017. Corresponding Editor: Debra P. C. Peters.

Copyright: © 2017 Swetnam et al. This is an open access article under the terms of the Creative Commons Attribution License, which permits use, distribution and reproduction in any medium, provided the original work is properly cited.

† **E-mail:** tswetnam@email.arizona.edu

INTRODUCTION

Mountains support 23% of global forests and 12% of the world's population (FAO 2016). Montane forests are an important continental-scale carbon sink (Schimel et al. 2001) and water supplier (Mote et al. 2005, Bales et al. 2006). These forests are also likely to experience significant negative impacts from anthropogenic climate change

(Beniston 2003, Millar et al. 2007). As regional climate warms and drought stress becomes more common, understanding how macroclimate and topography interact to influence montane forest carbon assimilation, respiration, and plant water-use efficiency become increasingly important (Brooks et al. 2011, 2015, Williams et al. 2013, Adams et al. 2014, Anderegg et al. 2015, McDowell and Allen 2015). Forest carbon uptake is

widely considered to increase along an elevation–climate environmental gradient where long growing seasons and large water availability coincide (Rosenzweig 1968, Whittaker and Niering 1975, Gholz 1982, Goulden et al. 1998). Underlying the elevation–climate gradient, complex terrain influences forest net primary production (NPP; Chen et al. 1999, Tague and Peng 2013, Brooks et al. 2015), sensitivity to insect mortality (Kaiser et al. 2013), and drought (Allen et al. 2015).

In complex terrain, slope aspect alters local energy balance (Gutiérrez-Jurado and Vivoni 2012), while subsurface geophysical structure alters groundwater availability (Tromp-van Meerveld and McDonnell 2006, Hu et al. 2009, Adams et al. 2014). For example, on equator-facing aspects, increased insolation results in more rapid melting and sublimation of snow and evaporation (Harpold et al. 2014a, Harpold 2016). Higher temperatures, as experienced on equator-facing aspects, can also result in larger respiration rates and less carbon sequestration in trees (Tromp-van Meerveld and McDonnell 2006, Hu et al. 2009).

Rainfall patterns in mountains are influenced by orographic lifting, which causes more rain to fall at high elevations relative to adjacent lower elevations (Broccoli and Manabe 1992). Complex terrain redistributes antecedent precipitation in the form of overland flow and as groundwater. Despite increases in precipitation at higher elevations, potential forest carbon uptake ultimately becomes temperature (energy) limited as atmospheric lapse rates reduce daily air temperatures below freezing for longer periods of the year (Hu et al. 2009, Bradford et al. 2010, Anderson-Teixeira et al. 2011, Knowles et al. 2014, Monson 2014, Monson and Baldocchi 2014). At lower elevation, forests become increasingly water limited as seen in western North American forests (Zapata-Rios et al. 2015).

Research focusing on the relationship between forest NPP to mean annual temperature (MAT) and mean annual precipitation (MAP) has found that climatic trends can be overwhelmed in complex terrain by the spatial redistribution (i.e., lateral flux) of precipitation along hydrological flow paths (Giardino and Houser 2005, Hu et al. 2009, McDonnell 2014, Brooks et al. 2015, Good et al. 2015). Emergent patterns in forest structure and size also reflect the variability in soil depth and soil water availability (Rango et al. 2006, Thompson

et al. 2011a, b, Hwang et al. 2012, Peterson and Lajtha 2013, Good et al. 2015). Smith et al. (2017) recently reported variability in forest carbon as being driven by slope aspect and topographic curvature in an eastern North American mixed-deciduous forest. Plant species richness and composition are also linked to topographic variation (Zinko et al. 2005, Kopecký and Cízková 2010, Moeslund et al. 2013). Conceptually, any hillslope can be divided into three zones (Brooks et al. 2015): toe slope and valley bottoms where plant available water is most likely to be subsidized from groundwater; transitional hillslopes that fluctuate in relative subsidy vs. precipitation; and upper slopes and ridges where plant available water is less than local precipitation as soil moisture and groundwater percolate downward and flow downslope (Stephenson 1990, Kaiser et al. 2013). Sensitivity of tree growth by topographic position to climate is one of the hallmarks of dendrochronological science (Fritts 1974, 1976), where growth is most sensitive on ridge and hillslope positions and least sensitive in valley bottoms. Redmond et al. (2017) recently demonstrated that piñon pine (*Pinus edulis*) were more sensitive to a difference in climate, that is summer vapor pressure deficit (VPD), on sites with high soil available water content.

The quantifiable effects of complex terrain on catchment-scale forest respiration, carbon uptake and storage, across an elevation-driven environmental gradient in water availability, are poorly understood. To address this knowledge gap, we compared forest aboveground carbon loading to topographic metrics describing energy balance and water availability across three headwater catchments to establish whether any consistent trends in topographic variation describe the distribution of biomass relative to the environmental–climate gradient.

MATERIALS AND METHODS

Study area

The Boulder Creek CZ Observatory Watershed is west of Boulder, Colorado, 40.03° N, 105.25° W (Fig. 1). The disturbance history of the three studied catchments: Como Creek, Gordon Gulch, and Betasso Preserve, is well understood, having been logged in the 19th century and preserved for the last century (Adams et al. 2014). The catchments contain second-growth forest, which

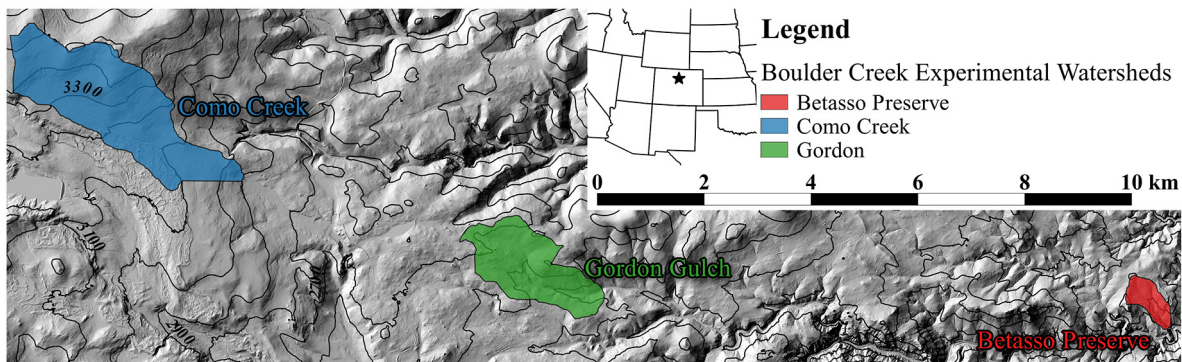


Fig. 1. Study area. Elevation in general decreases from left to right. The three catchments are colored blue (Como Creek), green (Gordon Gulch), and red (Betasso Preserve). For consistency, the color scheme is the same in all figures.

in Como are over 100 yr old (Knowles et al. 2014) and in Gordon Gulch approximately 160 yr old (Adams et al. 2014). Elevations range from 3560 meters (m) above mean sea level (a_{msl}) along the crest of Como Creek, down to 1810 m a_{msl} at the stream outlet of Betasso Preserve (Figs. 1 and 2, Table 1). Mean annual precipitation ranges from 1020 mm/yr at the highest elevations down to 460 mm/yr at the lowest (PRISM 2004, Hinckley et al. 2012). Physical descriptions of the entire Boulder Creek CZO are found at: <http://czo.colorado.edu/html/sites.shtml>, and climate observations are available at: <http://czo.colorado.edu/html/data-climate.shtml>.

Como Creek.—The most westerly, largest, and highest elevation catchment (Figs. 1 and 2, Table 1). The lithology is Paleoproterozoic biotite gneiss, Precambrian granite, granodiorite, and

monzonite. Soils are sandy loam inceptisols on biotite gneiss with talus in higher elevations above treeline (Dethier and Lazarus 2006, Berryman et al. 2015). This analysis only includes the 80% of Como Creek that is below treeline containing a mix of sub-alpine fir (*Abies lasiocarpa*), Engelmann spruce (*Picea engelmannii*), Lodgepole pine (*Pinus contorta*), limber pine (*Pinus flexilis*), and quaking aspen (*Populus tremuloides*; Rollins and Frame 2006; Appendix S1: Table S1).

Gordon Gulch.—The centrally located, mid-sized, and the mid-elevation catchment with the creek flowing approximately southeast (Figs. 1 and 2, Table 1). The lithology is Paleoproterozoic biotite gneiss, Precambrian granite, granodiorite, and monzonite. Deep soil profiles of Tertiary soil and rock erosion up to 15 m deep are present (Dethier and Lazarus 2006, Befus et al. 2011,

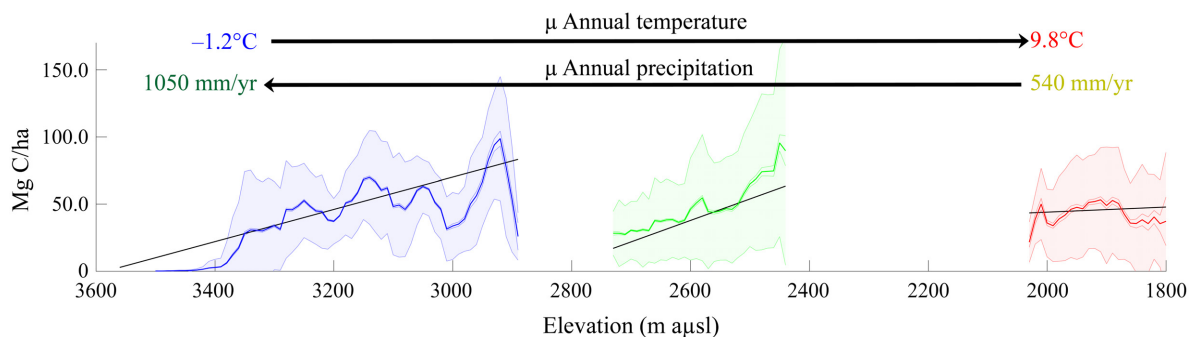


Fig. 2. Elevation vs. mean carbon. Distribution of the mean (μ , colored line), standard error about the mean (\pm SEM, darker shade), and first standard deviation ($\pm 1\sigma$, lighter wider shade) in aboveground C (Mg C/ha) by elevation (m a_{msl}). The black line is a linear regression.

Table 1. Study area physical descriptions and climatology.

Metric	Como Creek	Gordon Gulch	Betasso Preserve
Elevation (m μ sl)	2900–3560	2446–2737	1810–2024
Area (ha)	664	357	45
MAT ($^{\circ}$ C)	1.0	6.1	12.3
MAP (mm/yr)	1020	500	460
% Snow	70	50	20

Note: MAP, mean annual precipitation; MAT, mean annual temperature.

Dethier et al. 2012). Soils are loamy and sandy alfisol on granodiorite colluvium (Dethier et al. 2012, Berryman et al. 2015). Vegetation is mainly lodgepole pine on northerly aspects and ponderosa pine (*Pinus ponderosa*) on southerly aspects (Rollins and Frame 2006; Appendix S1: Table S1).

Betasso Preserve.—The most easterly, the smallest and lowest elevation catchment with the main drainage flowing to the southeast (Figs. 1 and 2, Table 1). The lithology is mostly decaying Laramide bedrock and saprolite with mobile upper regolith layer. Soils are loamy sandy alfisol on granodiorite colluvium (Dethier et al. 2012, Berryman et al. 2015). Vegetation is mostly ponderosa pine on south aspects and a mix of ponderosa pine and Douglas-fir (*Pseudotsuga menziesii* var. *glauca*) on north aspects (Rollins and Frame 2006; Appendix S1: Table S1).

Aerial lidar data

Snow-off, leaf-on discrete return aerial lidar data were collected over Boulder Creek CZ by the National Center for Airborne Laser Mapping (NCALM; <http://www.ncalm.org>) in June 2010 (Anderson et al. 2012). The lidar data have an average pulse density of 11.2 points per meter square and were collected with a 50% sidelap. The lidar data are consistent with United States Geological Survey (USGS) Base Specification Quality Level 1 (Heidemann 2014). The Boulder Creek snow-off lidar data are available via <http://www.opentopography.org>. Discrete pulse return data were processed into one-third meter square pixel, 0.333 m, digital elevation models (DEM) and digital surface models (DSM) using the OpenTopography “DEM Generation TIN” (triangular irregular network) and “Local Gridding” tools. Canopy height models (CHM) were generated by subtracting the DSM from the DEM (Lefsky et al. 2002, Zhao and Popescu 2007; Appendix S2: Figs. S1 and S2).

Aboveground biomass and carbon content

Individual tree biomass/carbon density was based on the dominant tree species classification, by the LANDFIRE existing vegetation type (EVT; Rollins and Frame 2006; Appendix S1: Table S1). Each tree was assigned an EVT in Quantum GIS (QGIS 2014 v2.8). The EVTs for all three catchments are mostly single species-dominant types (Appendix S1: Table S1). Wood specific gravity (SG, Chojnacky et al. 2014) and woody C content (%; Lamtom and Savidge 2003) values (Appendix S1: Table S2) were assigned for each EVT based on species. In the case of mixed-species forests, an average value was assigned. In the study areas, species variations in SG and C were typically $\pm 3\%$ of each other.

An individual tree segmentation script (Swetnam and Falk 2014) identified trees from the 0.333 m CHM in Matlab 2015a (Mathworks 2015; Appendix S2: Figs. S1 and S2). The script employed a minimum height cutoff of 2 m above ground level and a minimum canopy ratio of 1/8th to height (Swetnam and Falk 2014). Output for each tree included tree height, major and minor axis of canopy diameter, equivalent canopy diameter, and canopy area. The model for estimating tree diameter at breast height (dbh_{est}) is based on Eq. 7 in Swetnam and Falk (2014): $dbh_{est} = \beta Ht / \bar{D}_{can}$ (1), where dbh is in units of centimeters (cm), β is a coefficient equal to 0.82, Ht is tree height (m), and D_{can} is the diameter of the canopy (m).

Conventional aboveground biomass equations (Chojnacky et al. 2014) in logistic form: $\ln(AGB) = \beta_0 + \beta_1 \ln(dbh)$ (2) are comparable to the pipe model (Savage et al. 2010, Bentley et al. 2013): $V = \pi r^2 \times Ht$ (3), where V is volume and r is the bole radius ($r = dbh/2$). In our analysis, we used the pipe model to estimate V . AGB is derived by multiplying the tree SG by V . AGC is determined by multiplying AGB by mean C density

(Lamloom and Savidge 2003, Chojnacky et al. 2014; Appendix S1: Fig. S1). We used Eq. 3 to first estimate individual tree V , and the LANDFIRE EVT (Rollins and Frame 2006) to determine species-specific SG and C content (Appendix S1: Table S2): $C = V \times SG \times C(4)$.

Jucker et al. (2017) recently developed a global general model for individual tree dbh and AGB based on canopy diameter and maximum height measurements from lidar. In Appendix S3, we compared our individual tree dbh and AGB models to the general models for gymnosperms by Jucker et al. (2017). We found the southwestern USA dbh model reported by Swetnam and Falk (2014) to be more accurate ($r^2 = 0.82$, RMSE = 6.6 cm) than the gymnosperm general model reported by Jucker et al. (2017; $r^2 = 0.78$, RMSE = 7.4 cm) for southwestern conifers. Jucker et al. (2017) tended to under-estimate dbh in large trees (Appendix S3: Figs. S1 and S2). Both methods report similar tree AGB when given the same set of measurements (Appendix S3: Fig. S5). For the AGB calculation, the two models had some variation about a mean of zero. The propagation of uncertainty was derived by summing known measurement and model errors (Chave et al. 2004, Dalponte and Coomes 2017, Jucker et al. 2017).

For each catchment, we inventory the overstory forest as seen by the lidar. Consequently, the sampling bias is expected to be near zero for overstory trees. Understory trees, on the other hand, are likely to be missed when they are present beneath large trees. The contribution of biomass to the total stand from small trees beneath large trees is very small relative to the biomass contribution of the large trees (Lutz et al. 2012, Swetnam et al. 2014). The uncertainty in the biomass/carbon density values is expected to have a normal distribution with a mean of zero. The presence of small trees beneath larger trees would suggest that our reported estimates are conservative, rather than over estimates of actual biomass.

To compare standing tree biomass (point-based) to landscape (area-based) estimates, we aligned the 10-m topographic rasters to the individual trees in QGIS using the Vector–Research Tools “Vector Grid” and Vector–Analysis Tools “Points in Polygon.” After the individual tree C (kg) was determined, 10-m pixel-level C was summed (kg C 100 m⁻²) for each topographic grid

pixel. Stem and topographic metrics for each of the three catchments are hosted via the Critical Zone Observatory data web service page: <http://search.criticalzone.org/>.

Project data, code, and a wiki were maintained using CyVerse (Merchant et al. 2016). Jetstream cloud computing cyberinfrastructure (Stewart et al. 2015) was used for uncertainty analyses in R and R-Studio (R-Studio Team 2015). The data and R code are available online and in the supporting information.

Topographic variables

Digital elevation model layers were analyzed in open-source geographic information system (GIS) software, which included QGIS (Savage et al. 2010) and System for Automated Geoscientific Analysis (SAGA v 2.1.2; Conrad et al. 2015). First-order topographic relief included (1) elevation (m amsl); (2) the hillslope’s angle of repose, that is, slope (in degrees [°] or radians [rad or °]) relative to a flat surface; and (3) the azimuth or aspect of exposure (° or °). Other derivative measures of topographic relief included hillslope normalized height (unitless ratio between 0 and 1; Böhner and Selige 2006, Dietrich and Böhner 2008) and the Topographic Position Index (TPI; Guisan et al. 1999, Weiss 2001).

Slope, aspect, and curvature.—Changes in slope aspect have an effect on the energy balance of the surface topography related to solar insolation of a flat surface. Topographic curvature is the second derivative of slope angle along a hillslope, a measure of the change in either a vertical, horizontal, or tangential profile relative to the surface (Alkhasawneh et al. 2013). The influence of topographic curvature on subsurface lateral water redistribution is less well studied than Topographic Wetness Index (TWI), but has been shown to influence erosion rates (Pelletier and Rasmussen 2009a, Hurst et al. 2012), soil depth (Pelletier and Rasmussen 2009b), and regolith production from crystalline bedrock (Rempe and Dietrich 2014). Topographic curvature can influence the availability of both surface runoff, soil depth, and soil moisture.

Slope aspect (°) and general curvature (unitless) were calculated using the SAGA Terrain Analysis—Morphometry “Slope, Aspect, and Curvature” tool (Conrad et al. 2015). Alkhasawneh et al. (2013) provide the descriptions and equations for the different types of curvature. Simply put, the

second derivative of a slope is calculated across a moving window where a flat surface is equal to 0, a convex (divergent) surface is >0 , and a concave (convergent) surface is <0 ; the output values are scale dependent upon the pixel length. Curvature of the profile (vertical plane) affects the velocity of water flowing across a surface influencing both erosion and deposition rates (Mitasova et al. 1996). Planiform (horizontal plane, equivalent to tangential curvature) describes whether water is flowing convergent into or divergent away from the pixel. The planiform and profile curvature are compared together as “general curvature” (Wood 1996, Alkhasawneh et al. 2013).

Topographic wetness index.—To quantify topographic variation in surface wetness, we can calculate the natural log of the upslope contributing or catchment area (m^2) divided by the tangent of slope ($^\circ$), which gives the TWI (Beven and Kirkby 1979, Beven 1997, Kirkby 1997). Topographic Wetness Index can be derived using an array of GIS algorithm techniques (Quinn et al. 1991, 1995, Sørensen et al. 2006). Crucially, the TWI does not fully describe the subsurface structure, although it does often correlate with subsurface processes (Grabs et al. 2009). Topographic Wetness Index influences the overall soil water available for plant respiration and growth. Indirectly, it affects the energy balance by altering overall evaporation and transpiration resulting in cooler sites due to latent heat exchange.

Topographic Wetness Index is produced as: $TWI = \ln(\alpha/\tan\beta)$ (5), where α is the upslope contributing area (m^2) flowing downward through a pixel (in units of length squared, m^2) and $\tan\beta$ is the tangent of slope β ($^\circ$) in radians. Catchment area for the DEMs was calculated using the D^∞ method (Quinn et al. 1995, Tarboton 1997) in the SAGA Terrain Analysis—Hydrology “Catchment Area (Recursive)” tool (Böhner and Selige 2006). Sørensen et al. (2006) suggest a multi-flow path technique as the most appropriate method for characterizing the response of TWI in ecological phenomena. Notably, other important features in complex terrain that are not considered by TWI, such as varying depth of soil (Pelletier and Rasmussen 2009b) or depth to groundwater, can be estimated from other topographic metrics such as curvature.

Topographic position index.—Topographic Position Index indicates a change in the total water

availability due to surface runoff and groundwater availability. Indirectly, it also relates to surface energy balance from direct insolation as lower topographic positions are expected to experience greater daily shading from local terrain. Topographic Position Index is a scale-dependent index describing the difference between topographic positions (Guisan et al. 1999, Weiss 2001). Lower topographic positions, for example, valley bottoms and stream channels, have negative TPI, while upper topographic positions, for example, ridges and peaks, have positive TPI.

The length size of the moving window and the weighting technique (e.g., inverse distance weighting) determines the index value. Topographic Position Index was calculated in SAGA Terrain Analysis—Morphometry > Topographic Position Index (Guisan et al. 1999). The execution used the default parameters (a 150-m moving window with inverse distance weighting). The scale of the moving window was appropriate based on the length size of ridge to valley distances for the study catchments.

Hillslope positions.—Slope height is similar to TPI in explaining energy balance, as well as the conceptual hydrologic zone model for overall water availability (Brooks et al. 2015). The relative heights and slope positions were calculated using the SAGA Terrain Analysis—Morphometry > Relative Heights and Slope Positions (Böhner and Selige 2006, Dietrich and Böhner 2008). The outputs included the normalized height (unitless), the ratio of height (m) above the channel to the ridge (values between 0 and 1). Normalized height is similar to TPI, but scaled. Hydrologic Zones 1 through 3 are defined as 0.0–0.333, 0.334–0.666, and 0.667–1.00, respectively.

Descriptive statistics

The uncertainty analysis for the individual tree estimates of biomass/carbon density was done in R with RStudio (RStudio 2015). We followed the same technique as Chave et al. (2004), and Jucker et al. (2017), where we calculated the propagation of uncertainty for both potential measurement errors and model error (Appendix S3).

We generated summary statistics for every 10-m pixel in each catchment in Matlab 2015a (Mathworks 2015). We organized the statistics by a grouping function [grpstats] to calculate the mean (μ), median, maximum, first standard deviation (1σ), standard error about the mean ($se\mu$),

and the upper 99th percentile or confidence interval (CI, 2.58σ) of C for a new observation for each topographic metric. We also fit a least-squares linear regression with Matlab's Curve Fitting Tool (cftool) to each distribution to determine the sign of change in C by topographic metric (Appendix S4: Tables S1–S5). The reported sem (or se_{μ}) is essentially the standard deviation for the estimate of the sample mean. The 1σ represents a range of uncertainty in the mean C for each described topographic variable.

RESULTS

Individual tree inventories

From the lidar canopy height models, a total of 17,286 overstory trees were identified in Betasso Preserve (~380 trees/ha), 178,469 trees in Gordon Gulch (~470 trees/ha), and 317,274 trees in Como Creek (~480 trees/ha). Aboveground C at the 10-m grid resolution (Fig. 2) is the sum of all trees' estimated C within each 10-m pixel (kg C/0.01 ha). The units for the individual pixels are converted to equivalent Mg C/ha notation in the figures for consistency.

For individual trees, the measurement uncertainty for aboveground C was $\pm 40\%$ (based on height $\pm 5\%$, canopy diameter $\pm 23\%$, specific gravity $\pm 8\%$, carbon $\pm 4\%$; Appendix S3). The allometric model uncertainty was $\pm 32\%$ (based on dbh_{est}). Total uncertainty is 166–59% of the reported AGC (Appendix S3). In general, the absolute measurement errors are greater for small trees and less for larger trees. The large uncertainty for canopy diameter is due in part to the high frequency of small trees and the fundamental sampling resolution (± 0.333 m) of the surface models. The error is expected to have a mean of zero (Appendix S3) and a standard deviation which is smaller than the standard deviation reported about the reported pixel-level mean values.

The number of trees per hectare (ha^{-1}) had no relationship with total aboveground C. There was also no correlation in the number of trees/ha and topographic position in any of the three catchments. The distribution of C on a per-pixel basis was dominated by the presence of very large trees, estimated to hold 1832 ± 798 kg C. There is a greater likelihood of under-estimating biomass than of overestimating it based on our models. This is due in part to under-measurement of height and

canopy diameter by the lidar, and under-reporting of small-diameter trees obscured by larger trees (Appendix S2). The wide range in spatial heterogeneity of forest structure within the catchments showed few areas of highly concentrated C (i.e., >1500 kg C per pixel equivalent to 150 Mg C/ha) across any continuous area >1.0 ha (Fig. 3). The maximum C values tend to cluster into small groups where one or more very large trees are measured within a single or several 10-m pixels.

The Niwot Ridge eddy covariance flux tower is located at the lower end of Como Creek catchment (Knowles et al. 2014). Hu et al. (2009) reported aboveground biomass around the flux tower as 22.41 kg/m² and 24.17 kg/m² between east and west transects (equivalent to ~112 and ~121 Mg C ha, respectively). For comparison, our 99th percentile estimate of C in the Como Creek along mid-slope positions was 100 Mg C ha, and in low-lying positions 153 Mg C ha (Table 2).

Elevation and slope aspect

Within each catchment, mean C declined as elevation increased (Fig. 2; Appendix S4: Table S1). The peak values of C for the 99% confidence interval (CI, 2.58σ), representing hotspots of productivity, were observed along the lower topographic locations, for example, creek bottoms and toe slopes (Fig. 3). At the highest elevation site, Como Creek, the forest carbon reservoir went to zero as the catchment crosses above alpine treeline (>3450 m a.s.l.; Appendix S2: Fig. S3). In Gordon Gulch (Fig. 3), we found a similar magnitude of C and regression slope vs. elevation as Como (Fig. 2). In Betasso Preserve (Appendix S2: Fig. S3), the lowest elevation catchment, mean C is largest at the mid-catchment elevation and declines slightly toward the lowest elevations (Fig. 2).

Carbon storage was on average 20–40 Mg C ha greater on N to NE aspects than on S to SW aspects, a pattern most pronounced in Como Creek, the highest elevation, coldest and wettest catchment. Betasso Preserve showed the weakest response in mean C with slope aspect (Fig. 4).

Topographic curvature

Negative curvatures (i.e., convergent positions) tended to have greater mean and peak C than positive curvatures for all three catchments (Fig. 5; Appendix S4: Table S2). Variation in C to general curvature is only apparent at longer

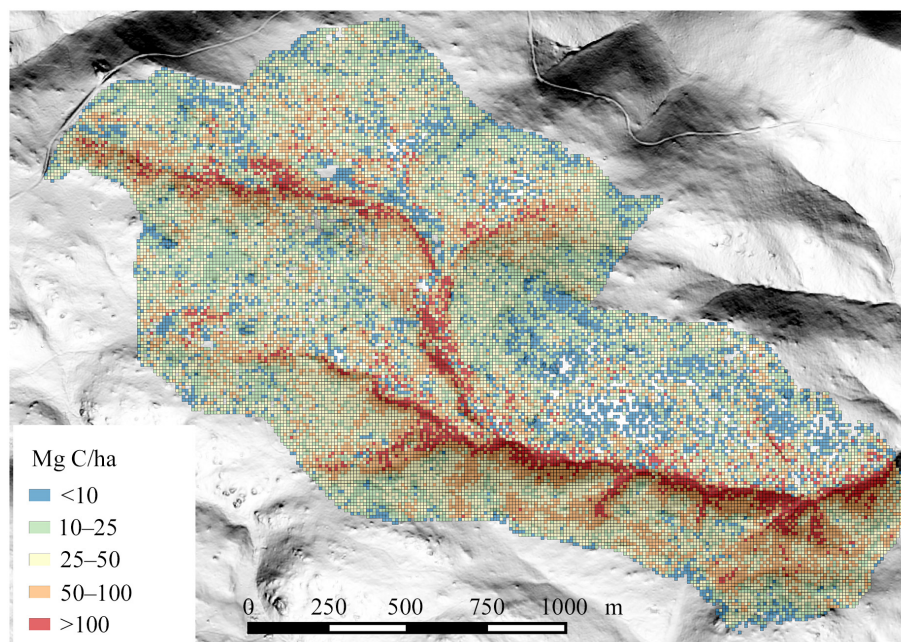


Fig. 3. Catchment mean carbon. Distribution of C for Gordon Gulch, aboveground C in equivalent units of Mg C/ha, shown for 10-m pixel size resolution. Surface is shaded from white (180° south facing) to black (0° north facing) with a 20 degree azimuth of insolation.

length scale (>10 m). At shorter length scale (1–5 m), the trend in C is lost due to micro-topographic changes, for example, the “noise” of root balls and tree boles pock marking the surface.

Hillslopes: normalized height and TPI

Catchment toe slopes and valleys held the largest mean and peak C values relative to transitional hillslope positions and ridges. Mean

aboveground C is greatest in the toe slopes and valley bottoms, and lowest on ridges, as measured using either normalized height (Fig. 6) or TPI (Fig. 7). In all three catchments, we found that mean forest carbon loading consistently increased from ridges (27 ± 19 Mg C ha) to valley bottoms (60 ± 28 Mg C ha). Low topographic positions held up to 185 ± 76 Mg C ha, more than twice the peak value of upper positions.

Table 2. Distribution of C (Mg C/ha) for the mean (μ) \pm standard error of the mean ($se\mu$), standard deviation ($\pm 1\sigma$), and upper 99% CI (2.58σ) classified into three zones in the three study catchments: toe slopes and valley bottoms (Zone 1), transitional hillslopes (Zone 2), and shoulder slopes and ridges (Zone 3).

Topographic Zone	Como Creek	Gordon Gulch	Betasso Preserve
	Mg C/ha		
Valleys ($\mu \pm se\mu$)	54 ± 1	59 ± 1	61 ± 1
Mid-slopes ($\mu \pm se\mu$)	28 ± 1	39 ± 1	45 ± 1
Ridges ($\mu \pm se\mu$)	13 ± 1	27 ± 1	30 ± 1
Valleys ($\pm 1\sigma$)	39	49	44
Mid-slopes ($\pm 1\sigma$)	28	28	30
Ridges ($\pm 1\sigma$)	19	19	24
Valleys (2.58σ)	153	185	174
Mid-slopes (2.58σ)	100	110	122
Ridges (2.58σ)	62	75	93

Note: The mean $\mu \pm se\mu$ and $\pm 1\sigma$ are shown in Fig. 6.

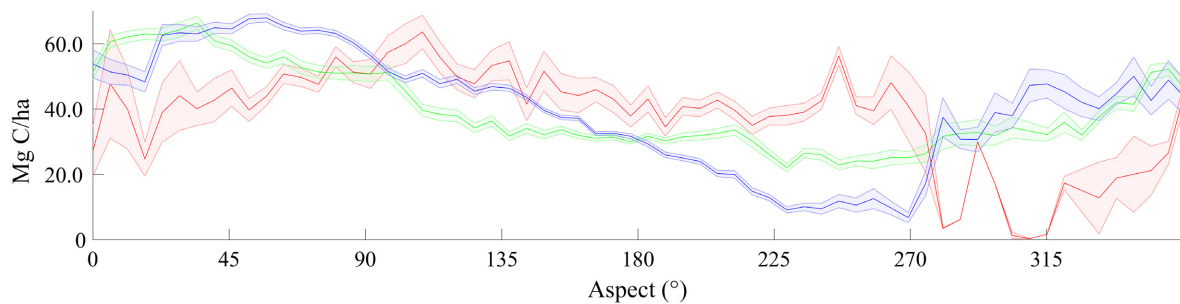


Fig. 4. Slope aspect vs. mean carbon. Distribution of the mean and standard error ($\mu \pm \text{SEM}$) in aboveground C (Mg C/ha) by aspect of exposure ($^{\circ}$). Betasso (red) has less variation in C in response to a change of aspect, while Como (blue) has the greatest and Gordon Gulch (green) is intermediate.

Among catchments, variation in mean C was equal to or greater when evaluated via topographic metrics than with the elevation–climate environmental gradient of MAT and MAP (Fig. 2). The mean C measure for all sites along valley bottoms vs. ridges was at least >101% larger using the normalized height metric (Fig. 6). The sem for most observed areas was small because of the large number of pixels from which the group statistics were generated (Table 2). The maximum value observed along a toe slope in Gordon Gulch was equivalent to 328 Mg C/ha; this is nearly an order of magnitude greater than the peak C values found along the top of the catchment of 34 Mg C/ha (Fig. 7). In Gordon Gulch, the peak distribution of C was strongly associated with landscape position; that is, areas near stream channels and north-facing aspects have the greatest aboveground C (Fig. 3).

Topographic wetness index

The differential response in C to TWI varied by catchment the most of any of our compared topographic variables (Fig. 8). Como had the weakest response having a weakly positive relationship. The response in Betasso, the most water-limited catchment, was the strongest, with greater than 100% increase in C from driest to wettest sites. In Gordon Gulch, there was an intermediate-state response to TWI, increasing by almost 50%.

DISCUSSION

The mean and maximum carbon loading in all three catchments varied relative to (1) the surface energy balance related to elevation and slope aspect and (2) four topographic proxies for lateral redistribution of soil water. Trends in C are the

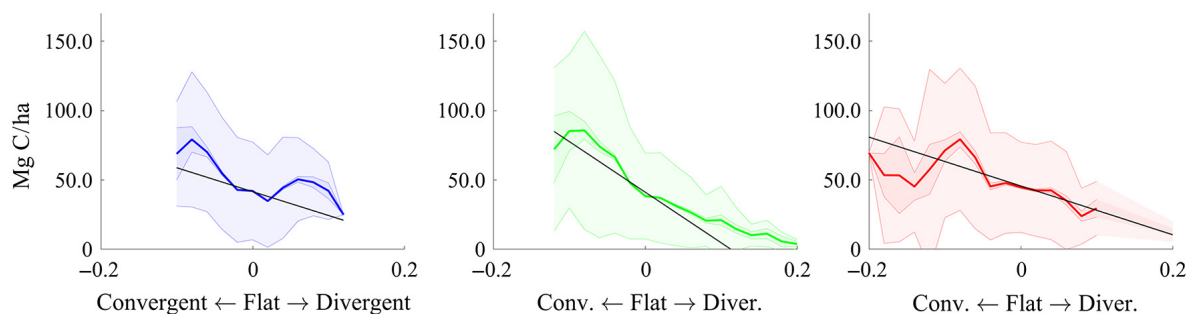


Fig. 5. Curvature vs. mean carbon. Distribution of the mean (μ , colored line), standard error about the mean ($\pm \text{SEM}$, darker shade), and first standard deviation ($\pm 1\sigma$, lighter wider shade) in aboveground C (Mg C/ha) vs. general curvature. The black line is a linear regression.

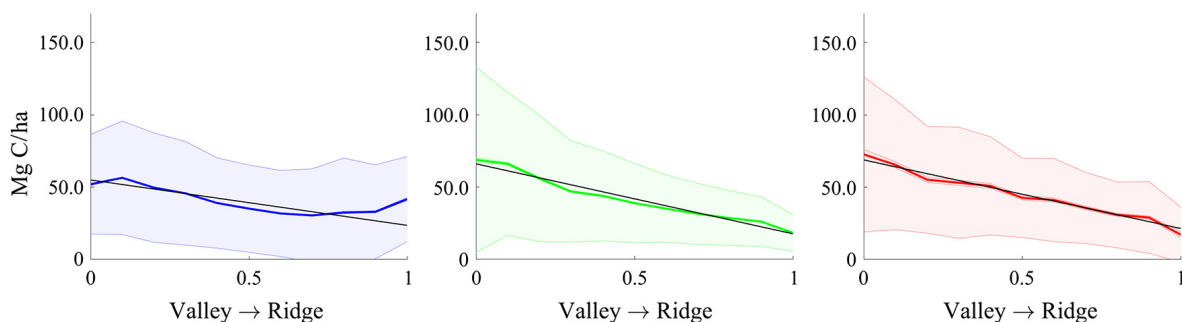


Fig. 6. Slope height vs. mean carbon. Distribution of the mean (μ , colored line), standard error about the mean (\pm SEM, darker shade), and first standard deviation ($\pm 1\sigma$, lighter wider shade) in aboveground C (Mg C/ha) vs. normalized slope height. The black line is a linear regression.

inverse of assumed elevation–climate environmental gradient responses with MAT and MAP (Appendix S5: Figs. S1 and S2). Rather than biomass increasing with lower (idealized) temperature and increased precipitation, the opposite trend is seen within catchments. In contrast to the environmental gradient hypothesis, related to long growing season length and abundant water availability, C was not significantly greater in the mid-elevation catchment relative to the other two catchments. We initially assumed the mid-elevation site would reflect a convergence of ideal temperature and water availability in relation to regional macroclimate and orographic effects. Instead, we found the sizes and patterns of the C reservoirs to be similar across catchments: From ridges to valleys, there was at least a 101% increase in the mean values, and there was a 146% increase in the peak values (Table 2, Fig. 3). Similarly, the

data show that variation in mean C with slope aspect in fact increases at higher elevations (lower MAT and higher MAP). North- and east-facing aspects had much more biomass than west- or south-facing aspects (Fig. 4) in Como Creek than in Betasso Preserve. We assumed at hotter lower elevations, trees on south aspects would experience greater evaporation and transpiration undergoing higher levels of respiration than those on north aspects at the same elevation. We also had assumed this trend would be reversed at higher elevation where lower air temperatures result in lower VPD on south aspects that are less water limited due to increased MAP, and that north aspects would become energy limited because of their near- or below-zero MAT resulting in less variation across slope aspect. The fact Como has greater variation in biomass on south aspects than on north aspects is surprising considering that the

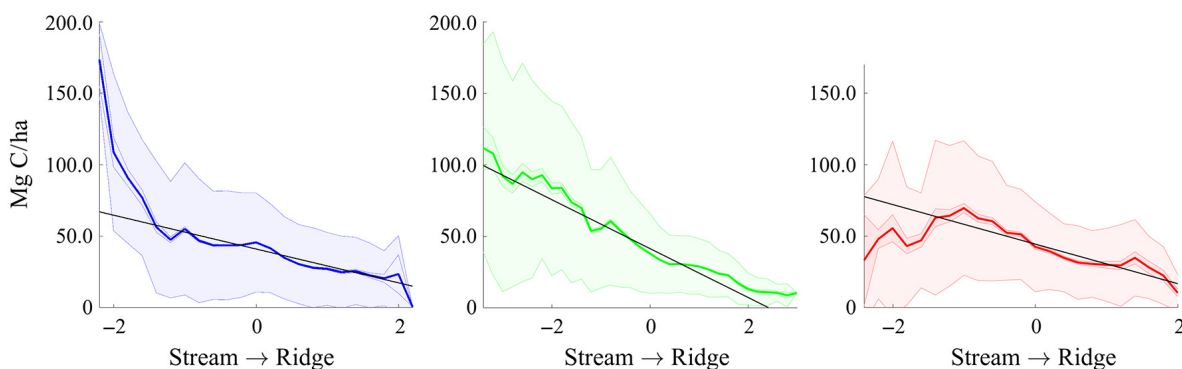


Fig. 7. Topographic Position Index vs. mean carbon. Distribution of the mean (μ , colored line), standard error about the mean (\pm SEM, darker shade), and first standard deviation ($\pm 1\sigma$, lighter wider shade) in aboveground C (Mg C/ha) vs. Topographic Position Index. The black line is a linear regression.

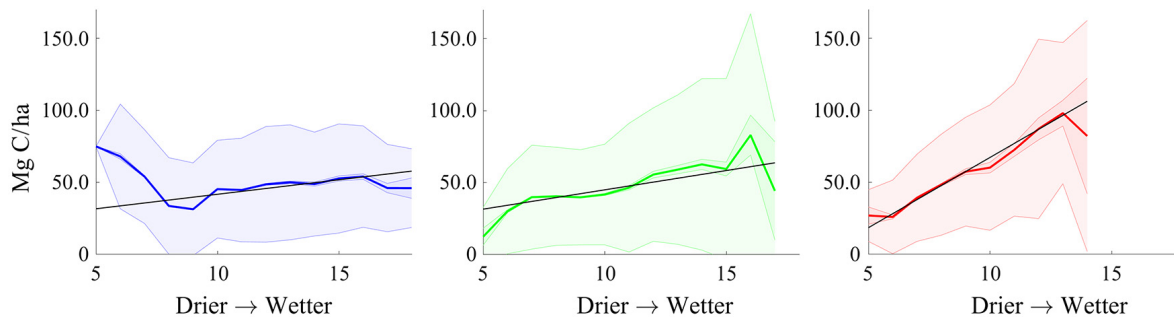


Fig. 8. Topographic Wetness Index vs. mean carbon. Distribution of the mean (μ , colored line), standard error about the mean (\pm SEM, darker shade), and first standard deviation (\pm 1 σ , lighter wider shade) in aboveground C (Mg C/ha) vs. Topographic Wetness Index. The black line is a linear regression.

catchment receives over one meter (>1000 mm/yr) of MAP and is thought to be periodically energy limited with shorter growing seasons (Hu et al. 2009, Knowles et al. 2015). We conjecture this greater biomass on north aspects may be a response to a decrease in snow sublimation and soil water evaporation on north aspects in the spring (Harpold et al. 2014a, b). Trees on north aspects may therefore be more likely to have snow water available to them when the growing season begins—even in drier hotter years. This trend was most pronounced in Como which receives the majority of its rainfall in the form of snow.

We were also initially concerned that variation in mean C may be exhibiting the residual impacts from logging which took place in the catchments in the late 19th and early 20th century. Adams et al. (2014) documented the location of scattered tree harvest primarily for fuelwood in Gordon Gulch, which we can see in our tree inventory data. Upon further examination, we found these stands to have slightly less C than unharvested locations; however, their small patch size did not significantly affect the overall trends seen in the catchment.

The response in mean and maximum C to a change in slope aspect is also likely to be partly controlled by the overall shape and direction of the basins. For example, Betasso is almost completely south and east facing with very few north-west-facing locations. Because the catchments are all predominantly eastward facing, this assumption requires additional tests in areas that predominantly face other cardinal directions.

There was a decrease in mean C for the most convergent locations in Betasso, which likely

corresponded to the steepest drainages at the bottom of the catchment having thinner soils and regolith as measured by seismic refraction (Befus et al. 2011, Knowles et al. 2015). Subsurface processes, such as soil depth and groundwater storage, are typically expressed at longer length scale, relating to ridge and valley sizes (Pelletier and Rasmussen 2009a). Some of the observed variation in C within the three catchments may relate to a change in soil depth and access to groundwater subsidy found in lower topographic positions.

Anecdotally, the largest local quantity of C was in the mid-elevation catchment, which met our assumption concerning the convergence of energy and water availability along the elevation gradient. However, the location is at the very bottom of the catchment, in a low topographic position. Carbon loading in Gordon Gulch exhibits a wide range in C, which underscores the importance of topography in establishing hotspots for productivity. The increased response of C to TWI values at lower, more water-limited elevation requires further study to determine whether surface flow and percolation or subsurface base flow are the dominant mechanism of lateral redistribution.

Further questions

Why was topographic position more important in explaining C storage than a doubling in MAP (± 500 mm) and 11°C change in MAT within these semi-arid forests? Other forest studies in complex terrain in humid (Smith et al. 2017), temperate (Buma et al. 2016, Zald et al. 2016), and tropical rain forest (Weintraub et al. 2015, Molina Simbaña

et al. 2016) have reported similar trends in biomass C accretion and decreases in nitrogen availability by hillslope position, suggesting a common pattern in even highly productive forest ecosystems. Our study is the first to consider the variability of carbon with a lateral redistribution in MAP across an elevation gradient in MAT. We show that trends in C are more consistently related to local topography than to climate. The most probable reasons in our study for an increase in C was the lateral redistribution of MAP to lower topographic positions, and variations in local energy balance with slope aspect, as posited by others (Hwang et al. 2012, Peterson and Lajtha 2013, Adams et al. 2014, McDonnell 2014, Brooks et al. 2015, Good et al. 2015). Maximum C in all three catchments appeared to be most related to topographic locations with (1) large upslope catchment area, (2) low slope angles, (3) negative general curvature (i.e., convergent positions), and (4) more northerly aspect of exposure. The observed increase in C, from ridges to valley bottoms, is further assumed to be at least partly a response to increased soil depth (Pelletier and Rasmussen 2009b, Hurst et al. 2012, Rempe and Dietrich 2014) and greater access to groundwater subsidy (Brooks et al. 2015).

Future research questions should focus on the processes driving C sequestration, as well as comparison to direct and indirect solar irradiation, nocturnal air flows, snow accumulation, inter-catchment groundwater transfer, changes in seasonality in MAP (e.g., the contribution of snow pack vs. summer precipitation to wetness) and VPD (e.g., the variation in local E/T relationships via differential exposure to solar heating and wind). Cold air pooling and nocturnal air flow (Yi et al. 2005, Dietrich and Böhner 2008) could have negative feedbacks on NPP and maximum C accumulation on lower topographic positions in higher-elevation, energy-limited catchments, and positive feedbacks on NPP and C for low-elevation, water-limited catchments (by lowering the daily VPD and E/T of local conditions). Knowles et al. (2015) found high-elevation catchments to fluctuate between energy limitation and water-limited states for wet and dry years, respectively. We did not specifically test the lateral redistribution of MAP across time in this study. The results do show that Como Creek and Gordon Gulch exhibit a greater response in C to slope aspect than Betasso

(Fig. 4). Meanwhile, Betasso exhibited the greatest response to changes in the lateral water redistribution (e.g., TWI), while Como Creek and Betasso exhibited a slightly negative to flat response (Fig. 6). This may point toward energy balance differences in MAP and E/T over time.

Broader implications

Recent studies indicate a trend toward more frequent and hotter droughts having an adverse effect on mountain forests (Allen et al. 2015). In particular, droughts more negatively affect taller trees than shorter trees (Williams et al. 2013, Anderegg et al. 2015, McDowell and Allen 2015). This study's approach at quantifying topographic controls on spatial patterns of C in trees highlights the importance of the lateral redistribution of water under warmer and drier conditions. Leading to the question: Does the lateral redistribution of water in complex terrain increase the sensitivity of trees or buffer them (as eco-hydrological refugia) from severe drought? Acutely, Adams et al. (2014) found that both *P. contorta* and *P. ponderosa* responded negatively to more water-limiting conditions mediated by the complex terrain in Gordon Gulch. At lower elevations in Colorado, Redmond et al. (2017) found that piñon pine on wetter sites responded more negatively to summer VPD in years with little winter precipitation. In relation to topographic position, Tague and Peng (2013) found that mid-slope positions are potentially the most sensitive to changes in water availability, describes the changing nature of sites on mid-slopes. Testable hypotheses related to carbon on mid-slope positions and increased sensitivity of vegetation to drought could be conducted using remotely sensed (i.e., lidar and hyperspectral imaging) data to determine tree stress and mortality vs. topographic position metrics including the hillslope normalized height and mid-slope index (Dietrich and Böhner 2008). Future models for predicting tree growth and survival (e.g., Williams et al. 2013, Anderegg et al. 2015, McDowell and Allen 2015) must take into account the non-linear effects of lateral redistribution of water in complex terrain if they wish to improve their prediction accuracy about where future tree mortality is likely to occur and what changes in the catchment-to-watershed-scale carbon and water cycle can be expected.

Lateral redistribution of plant available water and variation in energy balance related to the local topography are more important in explaining peak and mean aboveground carbon than an 11°C range in temperature and doubling of local precipitation related to the elevation–climate gradient. Specifically, toe slopes foster disproportionately high net carbon uptake. Spatially explicit models of tree-level processes, for example, respiration and total carbon uptake, must take into account the influences of local topography. Such models will be more likely to predict forest health and tree death as related to hydraulic failure and carbon starvation (e.g., Anderegg et al. 2015, McDowell and Allen 2015) than models that rely on climate variables alone.

In the absence of more information, a simple three-zone model (Brooks et al. 2015) can be used to normalize the expected distribution of potential forest C based on local microsite conditions. Variation in aboveground C in complex terrain not tied to MAT and MAP could have profound effects on published estimates of global NPP (Nemani et al. 2003) and regional to global estimates of mountain carbon reservoir size (Luysaert et al. 2008, Pan et al. 2011). These findings could also help to improve efforts into establishing forest drought stress, mortality, and overall carbon sequestration from remote sensing.

ACKNOWLEDGMENTS

We thank two anonymous reviewers and the subject editor for their comments that greatly improved the manuscript. Lidar data acquisition and processing were completed by the National Center for Airborne Laser Mapping (NCALM—<http://www.ncalm.org>), Project Director Qinghua Guo, collection for Dr. Suzanne Anderson (University of Colorado/INSTAAR, Boulder) as part of the Boulder Creek Critical Zone Observatory (CZO—<http://czo.colorado.edu/>), funded by National Science Foundation (NSF-0724960). NCALM funding was provided by NSF's Division of Earth Sciences, Instrumentation and Facilities Program EAR-1043051. This material is based upon work supported by the National Science Foundation under Award Numbers DBI-0735191 and DBI-1265383. URL: www.cyverse.org and Jetstream (144506) resources. Additional support was provided by the U.S. Department of Energy's Terrestrial Ecosystem Science Program (DOE Award no.: DE-SC0006968). T.L. Swetnam was also supported by the Santa Catalina-Jemez River Basin CZO (NSF-1331408).

LITERATURE CITED

- Adams, H. R., H. R. Barnard, and A. K. Loomis. 2014. Topography alters tree growth-climate relationships in a semi-arid forested catchment. *Ecosphere* 5:art148.
- Alkhasawneh, M. S., U. K. Ngah, L. T. Tay, and N. A. M. Isa. 2013. Determination of importance for comprehensive topographic factors on landslide hazard mapping using artificial neural network. *Environmental Earth Sciences* 72:787–799.
- Allen, C. D., D. D. Breshears, and N. G. McDowell. 2015. On underestimation of global vulnerability to tree mortality and forest die-off from hotter drought in the Anthropocene. *Ecosphere* 6:art129.
- Anderegg, W. R., A. Flint, C. Y. Huang, L. Flint, J. A. Berry, F. W. Davis, J. S. Sperry, and C. B. Field. 2015. Tree mortality predicted from drought-induced vascular damage. *Nature Geoscience* 8:367–371.
- Anderson, S. P., G. Qinghua, and E. G. Parrish. 2012. Snow-on and snow-off lidar point cloud data and digital elevation models for study of topography, snow, ecosystems and environmental change at Boulder Creek Critical Zone Observatory. Boulder Creek CZO, INSTAAR, University of Colorado at Boulder, Colorado, USA. <https://doi.org/10.5069/G93R0QR0>
- Anderson-Teixeira, K. J., J. P. Delong, A. M. Fox, D. A. Brese, and M. E. Litvak. 2011. Differential responses of production and respiration to temperature and moisture drive the carbon balance across a climatic gradient in New Mexico. *Global Change Biology* 17:410–424.
- Bales, R. C., J. W. Hopmans, A. T. O'Geen, M. Meadows, P. C. Hartsough, P. Kirchner, C. T. Hunsaker, and D. Beaudette. 2006. Mountain hydrology of the western United States. *Water Resources Research* 42:W08432. <https://doi.org/10.1029/2005WR00438>
- Befus, K. M., A. F. Sheehan, M. Leopold, S. P. Anderson, and R. S. Anderson. 2011. Seismic constraints on critical zone architecture, Boulder Creek watershed, Front Range, Colorado. *Vadose Zone Journal* 10:915–927.
- Beniston, M. 2003. Climatic change in mountain regions: a review of possible impacts. *Climatic change* 59:5–31. <https://doi.org/10.1023/A:1024458411589>
- Bentley, L. P., J. C. Stegen, V. M. Savage, D. D. Smith, E. I. Allmen, J. S. Sperry, P. B. Reich, and B. J. Enquist. 2013. An empirical assessment of tree branching networks and implications for plant allometric scaling models. *Ecology Letters* 16:1069–1078.
- Berryman, E., H. R. Barnard, H. R. Adams, M. A. Burns, E. Gallo, and P. D. Brooks. 2015. Complex terrain alters temperature and moisture limitations

- of forest soil respiration across a semiarid to subalpine gradient. *Journal of Geophysical Research: Biogeosciences* 120:707–723.
- Beven, K. J. 1997. TOPMODEL: a critique. *Hydrological Processes* 11:1069–1085.
- Beven, K. J., and M. J. Kirkby. 1979. A physically based, variable contributing area model of basin hydrology. *Hydrological Science Bulletin* 24:43–69.
- Böhner, J., and T. Selige. 2006. Spatial prediction of soil attributes using terrain analysis and climate regionalisation. SAGA-Analysis and modelling applications, Pages 13–28 *in* J. Böhner, K. R. McCloy, and J. Strobl, editors. *Göttinger Geographische Abhandlungen*, Göttingen, Germany.
- Bradford, J. B., P. Weishampel, M. L. Smith, R. Kolka, R. A. Birdsey, S. V. Ollinger, and M. G. Ryan. 2010. Carbon pools and fluxes in small temperate forest landscapes: variability and implications for sampling design. *Forest Ecology & Management* 259:1245–1254.
- Broccoli, A. J., and S. Manabe. 1992. The effects of orography on midlatitude Northern Hemisphere dry climates. *Journal of Climate* 5:1181–1201.
- Brooks, P. D., J. Chorover, Y. Fan, S. E. Godsey, R. M. Maxwell, J. P. McNamara, and C. Tague. 2015. Hydrological partitioning in the critical zone: recent advances and opportunities for developing transferrable understanding of water cycle dynamics. *Water Resources Research* 51:6973–6987.
- Brooks, P. D., P. A. Troch, M. Durcik, E. Gallo, and M. Schlegel. 2011. Quantifying regional scale ecosystem response to changes in precipitation: Not all rain is created equal. *Water Resources Research* 47:W00J08. <https://doi.org/10.1029/2010WR009762>
- Buma, B., K. Krapek, and R. T. Edwards. 2016. Watershed-scale forest biomass distribution in a perhumid temperate rainforest as driven by topographic, soil, and disturbance variables. *Canadian Journal of Forest Research*. <https://doi.org/10.1139/cjfr-2016-0041>
- Chave, J., R. Condit, S. Aguilar, A. Hernandez, S. Lao, and R. Perez. 2004. Error propagation and scaling for tropical forest biomass estimates. *Philosophical Transactions of the Royal Society B: Biological Sciences* 359:409–420.
- Chen, J., S. C. Saunders, T. R. Crow, R. J. Naiman, K. D. Broszofsky, G. D. Mroz, B. L. Brookshire, and J. F. Franklin. 1999. Microclimate in forest ecosystem and landscape ecology variations in local climate can be used to monitor and compare the effects of different management regimes. *BioScience* 49:288–297.
- Chojnacky, D. C., L. S. Heath, and J. C. Jenkins. 2014. Updated generalized biomass equations for North American tree species. *Forestry* 87:129–151.
- Conrad, O., B. Bechtel, M. Bock, H. Dietrich, E. Fischer, L. Gerlitz, J. Wehberg, V. Wichmann, and J. Böhner. 2015. System for automated geoscientific analyses SAGA. v. 2.1.4. *Geoscientific Model Development Discussions* 8:2271–2312.
- Dalponte, M., and D. A. Coomes. 2016. Tree-centric mapping of forest carbon density from airborne laser scanning and hyperspectral data. *Methods in Ecology and Evolution* 7:1236–1245.
- Dethier, D. P., P. W. Birkeland, and J. A. McCarthy. 2012. Using the accumulation of CBD-extractable iron and clay content to estimate soil age on stable surfaces and nearby slopes, Front Range, Colorado. *Geomorphology* 173:17–29.
- Dethier, D. P., and E. D. Lazarus. 2006. Geomorphic inferences from regolith thickness, chemical denudation and CRN erosion rates near the glacial limit, Boulder Creek catchment and vicinity, Colorado. *Geomorphology* 75:384–399.
- Dietrich, H., and J. Böhner. 2008. Cold air production and flow in a low mountain range landscape in Hessa Germany. SAGA—Seconds Out, Hamburger Beiträge Zur Physischen Geographie Und Landschaftsökologie, University Hamburg, Institut für Geographie, Hamburg, 37–48.
- Food and Agriculture Organization, United Nations. 2016. State of the World's Forests 2016. <http://www.fao.org/publications/sofo/en/>
- Fritts, H. C. 1974. Relationships of ring widths in arid site conifers to variation in monthly temperature and precipitation. *Ecological Monographs* 44:411–440.
- Fritts, H. C. 1976. *Tree rings and climate*. Academic Press Inc., London, UK, pp. 566.
- Gholz, H. L. 1982. Environmental limits on above-ground net primary production, leaf area, and biomass in vegetation zones of the Pacific Northwest. *Ecology* 63:469–481.
- Giardino, J. R., and C. Houser. 2015. *Principles and dynamics of the critical zone*. Volume 19. Elsevier Publishing, Oxford, UK.
- Good, S. P., D. Noone, and G. Bowen. 2015. Hydrologic connectivity constrains partitioning of global terrestrial water fluxes. *Science* 349:175–177.
- Goulden, M. L., et al. 1998. Sensitivity of boreal forest carbon balance to soil thaw. *Science* 279:214–217.
- Grabs, T., J. Seibert, K. Bishop, and H. Laudon. 2009. Modeling spatial patterns of saturated areas: A comparison of the topographic wetness index and a dynamic distributed model. *Journal of Hydrology* 373:15–23.
- Guisan, A., S. B. Weiss, and A. D. Weiss. 1999. GLM versus CCA spatial modeling of plant species distribution. *Plant Ecology* 143:107–122.
- Gutiérrez-Jurado, H. A., and E. R. Vivoni. 2012. Ecogeomorphic expressions of an aspect-controlled

- semiarid basin: II. Topographic and vegetation controls on solar irradiance. *Ecohydrology* 6: 24–37.
- Harpold, A. 2016. Diverging sensitivity of soil water stress to changing snowmelt timing in the Western U.S. *Advances in Water Resources*. <https://doi.org/10.1016/j.advwatres.2016.03.017>
- Harpold, A. A., N. P. Molotch, K. N. Musselman, R. C. Bales, P. B. Kirchner, M. Litvak, and P. D. Brooks. 2014a. Soil moisture response to snowmelt timing in mixed-conifer subalpine forests. *Hydrological Processes* 29:2782–2798.
- Harpold, A. A., et al. 2014b. Lidar-derived snowpack data sets from mixed conifer forests across the Western United States. *Water Resources Research* 50:2749–2755.
- Heidemann, H. K. 2014. Lidar base specification (ver. 1.2, November 2014): U.S. Geological Survey Techniques and Methods, book 11, chap. B4, 67 p. with appendixes, <https://doi.org/10.3133/tm11B4>
- Hinckley, E. L. S., B. A. Ebel, R. T. Barnes, R. S. Anderson, M. W. Williams, and S. P. Anderson. 2012. Aspect control of water movement on hillslopes near the rain-snow transition of the Colorado Front Range. *Hydrological Processes* 28:74–85.
- Hu, W., M. Shao, Q. Wang, J. Fan, and R. Horton. 2009. Temporal changes of soil hydraulic properties under different land uses. *Geoderma* 149:355–366.
- Hurst, M. D., S. M. Mudd, R. Walcott, M. Attal, and K. Yoo. 2012. Using hilltop curvature to derive the spatial distribution of erosion rates. *Journal of Geophysical Research* 117:F02017.
- Hwang, T., L. E. Band, T. M. Vose, and C. Tague. 2012. Ecosystem processes at the watershed scale: hydrologic vegetation gradient as an indicator for lateral hydrologic connectivity of headwater catchments. *Water Resources Research* 48:W06514. <https://doi.org/10.1029/2011WR011301>
- Jucker, T., et al. 2017. Allometric equations for integrating remote sensing imagery into forest monitoring programmes. *Global Change Biology* 23:177–190.
- Kaiser, K. E., B. L. McGlynn, and R. E. Emanuel. 2013. Ecohydrology of an outbreak: Mountain pine beetle impacts trees in drier landscape positions first. *Ecohydrology* 6:444–454.
- Kirkby, M. J. 1997. TOPMODEL: a personal view. *Hydrological Processes* 11:1087–1097.
- Knowles, J. F., S. P. Burns, P. D. Blanken, and R. K. Monson. 2014. Fluxes of energy, water, and carbon dioxide from mountain ecosystems at Niwot Ridge, Colorado. *Plant Ecology & Diversity* 1–14. <https://doi.org/10.1080/17550874.2014.904950>
- Knowles, J. F., A. A. Harpold, R. Cowie, M. Zeliff, H. R. Barnard, S. P. Burns, P. D. Blanken, J. F. Morse, and M. W. Williams. 2015. The relative contributions of alpine and subalpine ecosystems to the water balance of a mountainous, headwater catchment. *Hydrological Processes* 29:4794–4808. <https://doi.org/10.1002/hyp.10526>
- Kopecký, M., and Š. Čížková. 2010. Using topographic wetness index in vegetation ecology: Does the algorithm matter? *Applied Vegetation Science* 13: 450–459.
- Lamblom, S. H., and R. A. Savidge. 2003. A reassessment of carbon content in wood: variation within and between 41 North American species. *Biomass and Bioenergy* 25:381–388.
- Lefsky, M. A., W. B. Cohen, G. G. Parker, and D. J. Harding. 2002. Lidar remote sensing for ecosystem studies. *BioScience* 52:19–30.
- Lutz, J. A., A. J. Larson, M. E. Swanson, and J. A. Freund. 2012. Ecological importance of large-diameter trees in a temperate mixed-conifer forest. *PLoS One* 7:e36131.
- Luyssaert, S., E. D. Schulze, A. Börner, A. Knohl, D. Hessenmöller, B. E. Law, P. Ciais, and J. Grace. 2008. Old-growth forests as global carbon sinks. *Nature* 455:213–215.
- Mathworks, Inc. 2015. MATLAB: the language of technical computing. Desktop tools and development environment, version R2015B. MathWorks, Natick, Massachusetts, USA.
- McDonnell, J. J. 2014. The two water worlds hypothesis: Ecohydrological separation of water between streams and trees? *Wiley Interdisciplinary Reviews: Water* 1:323–329.
- McDowell, N. G., and C. D. Allen. 2015. Darcy's law predicts widespread forest mortality under climate warming. *Nature Climate Change* 5:669–672.
- Merchant, N., E. Lyons, S. Goff, M. Vaughn, D. Ware, D. Micklos, and P. Antin. 2016. The iPlant collaborative: cyberinfrastructure for enabling data to discovery for the life sciences. *PLoS Biology* 14: e1002342.
- Millar, C. I., N. L. Stephenson, and S. L. Stephens. 2007. Climate change and forests of the future: managing in the face of uncertainty. *Ecological Applications* 17:2145–2151.
- Mitasova, H., J. Hofierka, M. Zlocha, and L. R. Iverson. 1996. Modelling topographic potential for erosion and deposition using GIS. *International Journal of Geographical Information Systems* 10:629–641.
- Moeslund, J. E., L. Arge, P. K. Bøcher, T. Dalgaard, R. Ejrnæs, M. V. Odgaard, and J. C. Svenning. 2013. Topographically controlled soil moisture drives plant diversity patterns within grasslands. *Biodiversity and Conservation* 22:2151–2166.
- Molina Simbaña, P. X., M. Farjas Abadía, J. C. Ojeda Manrique, L. A. Sánchez Diez, G. Asner, and

- R. Valencia. 2016. Spatially-explicit testing of a general aboveground carbon density estimation model in a western Amazonian forest using airborne lidar. *Remote Sensing* 8:9.
- Monson, R. K. 2014. Ecology of temperate forests. *Ecology and Environment* 273–296.
- Monson, R. K., and D. Baldocchi. 2014. Terrestrial biosphere-atmosphere fluxes. Cambridge University Press, Cambridge, UK, pp. 488.
- Mote, P. W., A. F. Hamlet, M. P. Clark, and D. P. Lettenmaier. 2005. Declining mountain snowpack in western North America. *Bulletin American Meteorological Society* 86:39–49.
- Nemani, R. R., C. D. Keeling, H. Hashimoto, W. M. Jolly, S. C. Piper, C. J. Tucker, R. B. Myneni, and S. W. Running. 2003. Climate-driven increases in global terrestrial net primary production from 1982 to 1999. *Science* 300:1560–1563.
- Pan, Y., et al. 2011. A large and persistent carbon sink in the world's forests. *Science* 333:988–993.
- Pelletier, J. D., and C. Rasmussen. 2009a. Quantifying the climatic and tectonic controls on hillslope steepness and erosion rate. *Lithosphere* 1:73–80.
- Pelletier, J. D., and C. Rasmussen. 2009b. Geomorphically based predictive mapping of soil thickness in upland watersheds. *Water Resources Research* 45: W09417. <https://doi.org/10.1029/2008WR007319>
- Peterson, F. S., and K. J. Lajtha. 2013. Linking aboveground net primary productivity to soil carbon and dissolved organic carbon in complex terrain. *Journal of Geophysical Research: Biogeosciences* 118:1225–1236.
- PRISM Climate Group, Oregon State University. 2004. <http://prism.oregonstate.edu>
- QGIS. 2014. Quantum GIS Geographic Information System. Open Source Geospatial Foundation Project. <http://qgis.osgeo.org>
- Quinn, P., K. Beven, P. Chevallier, and O. Planchon. 1991. The prediction of hillslope flow paths for distributed hydrological modeling using digital terrain models. *Hydrological Processes* 5:59–80.
- Quinn, P., K. Beven, and R. Lamb. 1995. The $\ln(a/\tan\beta)$ index: how to calculate it and how to use it within the Topmodel framework. *Hydrological Processes* 9:161–182.
- Rango, A., S. L. Tartowski, A. Laliberte, J. Wainwright, and A. Parsons. 2006. Islands of hydrologically enhanced biotic productivity in natural and managed arid ecosystems. *Journal of Arid Environments* 65:235–252.
- Redmond, M. D., K. C. Kelsey, A. K. Urza, and N. N. Barger. 2017. Interacting effects of climate and landscape physiography on piñon pine growth using an individual-based approach. *Ecosphere* 8: e01681. <https://doi.org/10.1002/ecs2.1681>
- Rempe, D. M., and W. E. Dietrich. 2014. A bottom-up control on fresh-bedrock topography under landscapes. *Proceedings of the National Academy of Sciences* 111:6576–6581.
- Rollins, M. G., and C. K. Frame, editors. 2006. The LANDFIRE Prototype Project: nationally consistent and locally relevant geospatial data for wildland fire management. Gen. Tech. Rep. RMRS-GTR-175. Forest Service, Rocky Mountain Research Station, Fort Collins, Colorado, USA.
- Rosenzweig, M. L. 1968. Net primary productivity of terrestrial communities: prediction from climatological data. *American Naturalist* 67–74.
- RStudio Team. 2015. RStudio: integrated development for R. RStudio, Inc., Boston, Massachusetts, USA. <http://www.rstudio.com/>
- Savage, V. M., L. P. Bentley, B. J. Enquist, J. S. Sperry, D. D. Smith, P. B. Reich, and E. I. Von Allmen. 2010. Hydraulic trade-offs and space filling enable better predictions of vascular structure and function in plants. *Proceedings of the National Academy of Sciences* 107:22722–22727.
- Schimel, D. S., et al. 2001. Recent patterns and mechanisms of carbon exchange by terrestrial ecosystems. *Nature* 414:169–172.
- Smith, L. A., D. M. Eissenstat, and M. W. Kaye. 2017. Variability in aboveground carbon driven by slope aspect and curvature in an eastern deciduous forest, USA. *Canadian Journal of Forest Research* 47:149–158.
- Sørensen, R., U. Zinko, and J. Seibert. 2006. On the calculation of the topographic wetness index: evaluation of different methods based on field observations. *Hydrology and Earth System Sciences Discussions* 10:101–112.
- Stephenson, N. L. 1990. Climatic control of vegetation distribution: the role of the water balance. *American Naturalist* 649–670.
- Stewart, C. A., et al. 2015. Jetstream: a self-provisioned, scalable science and engineering cloud environment. In *Proceedings of the 2015 XSEDE Conference: scientific Advancements Enabled by Enhanced Cyberinfrastructure*. St. Louis, Missouri. ACM: 2792774. Pages 1–8.
- Swetnam, T. L., and D. A. Falk. 2014. Application of metabolic scaling theory to reduce error in local maxima tree segmentation from aerial lidar. *Forest Ecology and Management* 323:158–167.
- Swetnam, T. L., D. A. Falk, A. M. Lynch, and S. R. Yool. 2014. Estimating individual tree mid-and understory rank-size distributions from airborne laser scanning in semi-arid forests. *Forest Ecology and Management* 330:271–282.
- Tague, C., and H. Peng. 2013. The sensitivity of forest water use to the timing of precipitation and

- snowmelt recharge in the California Sierra: implications for a warming climate. *Journal of Geophysical Research: Biogeosciences* 118:875–887.
- Tarboton, D. G. 1997. A new method for the determination of flow directions and upslope areas in grid digital elevation models. *Water Resources Research* 33:309–319.
- Thompson, S. E., C. J. Harman, A. G. Konings, M. Sivapalan, A. Neal, and P. A. Troch. 2011b. Comparative hydrology across AmeriFlux sites: the variable roles of climate, vegetation, and groundwater. *Water Resources Research* 47:W00J07.
- Thompson, S. E., C. J. Harman, P. A. Troch, P. D. Brooks, and M. Sivapalan. 2011a. Spatial scale dependence of ecohydrologically mediated water balance partitioning: a synthesis framework for catchment ecohydrology. *Water Resources Research* 47:W00J03. <https://doi.org/10.1029/2010WR009998>
- Tromp-van Meerveld, H. J., and J. J. McDonnell. 2006. On the interrelations between topography, soil depth, soil moisture, transpiration rates and species distribution at the hillslope scale. *Advances in Water Resources* 29:293–310.
- Weintraub, S. R., P. G. Taylor, S. Porder, C. C. Cleveland, G. P. Asner, and A. R. Townsend. 2015. Topographic controls on soil nitrogen availability in a lowland tropical forest. *Ecology* 96:1561–1574.
- Weiss, A. D. 2001. Topographic position index and landform analysis. ESRI Users Conference, San Diego, California, USA. http://www.jennessent.com/downloads/TPI-poster-TNC_18x22.pdf
- Whittaker, R. H., and W. A. Niering. 1975. Vegetation of the Santa Catalina Mountains, Arizona. V. Biomass, production, and diversity along the elevation gradient. *Ecology* 56:771–790. <https://doi.org/10.2307/1936291>
- Williams, A. P., et al. 2013. Temperature as a potent driver of regional forest drought stress and tree mortality. *Nature Climate Change* 3:292–297.
- Wood, J. D. 1996. The geomorphological characterisation of digital elevation model. Dissertation. University of Leicester, Leicester, UK. <http://www.soi.city.ac.uk/~jwo/phd/>
- Yi, C., R. K. Monson, Z. Zhai, D. E. Anderson, B. Lamb, G. Allwine, A. A. Turnipseed, and S. P. Burns. 2005. Modeling and measuring the nocturnal drainage flow in a high-elevation, subalpine forest with complex terrain. *Journal of Geophysical Research: Atmospheres* 110:D22303. <https://doi.org/10.1029/2005JD006282>
- Zald, H. S., T. A. Spies, R. Seidl, R. J. Pabst, K. A. Olsen, and E. A. Steel. 2016. Complex mountain terrain and disturbance history drive variation in forest aboveground live carbon density in the western Oregon Cascades, USA. *Forest Ecology and Management* 366:193–207.
- Zapata-Rios, X., J. McIntosh, L. Rademacher, P. A. Troch, P. D. Brooks, C. Rasmussen, and J. Chorover. 2015. Climatic and landscape controls on water transit times and silicate mineral weathering in the critical zone. *Water Resources Research* 51:6036–6051.
- Zhao, K., and S. Popescu. 2007. Hierarchical watershed segmentation of canopy height model for multi-scale forest inventory. Proceedings of the ISPRS Working Group Laser Scanning 436–442. http://ssl.tamu.edu/media/14506/zhao_popescu_2007_international_archives_prs.pdf
- Zinko, U., J. Seibert, M. Dynesius, and C. Nilsson. 2005. Plant species numbers predicted by a topography based groundwater-flow index. *Ecosystems* 8:430–441.

SUPPORTING INFORMATION

Additional Supporting Information may be found online at: <http://onlinelibrary.wiley.com/doi/10.1002/ecs2.1797/full>